

# **A Systems Biology view of Breast cancer via Fractal Geometry and Fractional Calculus**

Abhijeet Das<sup>1,\*</sup>, Ramray Bhat<sup>1,2</sup>, Mohit Kumar Jolly<sup>1</sup>

<sup>1</sup>Department of Bioengineering, Indian Institute of Science, Bangalore – 560012, India

<sup>2</sup>Department of Developmental Biology and Genetics, Indian Institute of Science, Bangalore  
– 560012, India

**\*Corresponding Author – [abhijeetdas@iisc.ac.in](mailto:abhijeetdas@iisc.ac.in)**

**Abstract:** Breast cancer (BC) is the most widespread cancer globally, yet current diagnostic and prognostic methods inadequately capture its biological complexity, despite the benefits of early detection. Cancer systems biology (SB) has advanced over the past two decades as a multiscale approach, but often neglects morphological complexity observable at cellular, tissue, and tumor levels. Structural organization significantly influences system behavior, necessitating the identification of scales where morphological features emerge. Fractal geometry (FG) provides quantitative tools to assess the irregular, scale-invariant structures typical of cancer. Alongside FG, fractional calculus (FC) offers a framework to model memory-dependent and non-local dynamics. However, existing research remains constrained to mono-fractal analyses or limited imaging scopes, lacking integration into broader SB models. This review aims to bridge that gap by presenting core FG concepts, both mono- and multi-fractal measures, and their application to BC across histological, cytological, and radiological data. It further explores how FC enhances dynamic morphological modeling. Finally, it considers how number-theoretic tools like p-adic analysis may represent hierarchical genomic and morphological patterns, unifying insights from tumor morphology to genome organization.

**Keywords:** Breast cancer, Cell, Complexity, Fractal Geometry, Fractional Calculus, Morphology, Systems Biology, Tissue, Tumour

## **1. Introduction:**

### **1.1 Global Burden of Breast Cancer:**

Breast cancer (BC) emerged as the leading global cancer in 2020 with approximately 2.3 million new cases, representing 11.7% of all cancer diagnoses and 7% of cancer-related deaths worldwide. It remains the most prevalent malignancy among women.<sup>1</sup> Early detection and prompt treatment constitute the most effective and economically viable control strategies.<sup>2</sup> Recognizing this imperative, the World Health Organization launched the Global Breast Cancer Initiative in March 2021, targeting a reduction in global BC mortality to 2.5% by 2040, with particular focus on supporting low- and middle-income countries through evidence-based technical assistance. Despite advances in molecular diagnostics and gene therapy, current statistics highlight the limitations of existing BC research approaches, emphasizing the need for more effective diagnostic tools through novel frameworks. This situation necessitates a paradigm shift in carcinogenesis interpretation, moving beyond strictly gene-centric reductionist perspectives.

### **1.2 Systems Biology Approach to Cancer:**

In the early part of the 21<sup>st</sup> century, Hornberg *et al.*<sup>3</sup> questioned whether the effects of genetic mutations could be meaningfully predicted if tumors and surrounding cells form a complex supracellular communication network, and if this is the case, then how should one approach identifying drug targets? In response, they emphasized recognition of cancer as an SB disease and suggested that cancer research might progress more effectively if investigated from an SB perspective rather than solely through molecular biology. This approach emphasizes not only computational modeling but also a fundamental shift in philosophy: moving beyond the reductionist gene-centric framework in favor of complex systems thinking. In other words, the approach advocates moving beyond the reductionist, gene-centric paradigm by incorporating additional levels of biological organization, such as cell and tissue morphology, microenvironmental dynamics, and spatial–temporal regulatory interactions, into the analysis and modeling of carcinogenesis. It accepts that the tension between these two views represents a critical barrier to the advancement of future medical therapies.<sup>4</sup> Here, the second view emphasizes multi-scale integration, linking genetic, epigenetic, morphological, and environmental factors into a coherent, dynamic system model of cancer progression. Nevertheless, implementing this shift in breast cancer research requires a solid understanding of the concepts of *systems* and *complex systems* in both general and biological contexts.

### **1.2.1 Limitation of Current Biological Paradigms:**

Modern biology has largely neglected biological entities as systems by failing to address problems across different observational levels. The central dogma's widespread acceptance has extended reductionist models to define life itself, focusing cancer research primarily on molecular entities like genes, enzymatic reactions, and intracellular pathways. However, biological systems transcend mere assemblies of genes and proteins, with properties beyond simple interconnection maps.<sup>5</sup> While thermodynamics defines systems as clearly bounded parts of the universe, this becomes problematic for biological systems since thermodynamics primarily addresses macroscopic variables through statistical descriptions of uncorrelated particles. In contrast, biological systems display highly correlated, organized structures where *shape* or *morphology* and *structure* cannot be ignored.

### **1.2.2 Mesoscopic Organization and Biological Complexity:**

Matter organization at the mesoscopic scale holds undiscovered principles underlying emergent properties.<sup>6</sup> In biological systems, shape refers to geometric configurations of cells and cellular assemblies, while structure denotes spatial organization and mechanical relationships between components. These features govern how forces, signals, and molecular gradients transmit across scales, making mesoscopic-level study, where dynamic interactions generate morphological features, critically important. At this level, physical form is not merely a consequence of genetic information but reflects the integration of internal and external constraints.<sup>7</sup> In this context, (1) while the genome represents a digital core of information,<sup>8</sup> it does not fully account for the emergent complexity or tissue-level behaviors of biological systems<sup>9</sup> and (2) a comprehensive system-level understanding requires a reorientation: rather than seeking single molecular causes, we must quantify and interpret multiscale patterns of morphological organization and their dynamic regulation..

Moreover, no simple correspondence exists between genes/proteins and higher-level biological functions.<sup>4</sup> The traditional prioritization of molecular-level explanations is biased, especially since *levels* itself is metaphorical in biology.<sup>10</sup> SB proposes a middle-ground approach to uncover self-organization rules at the mesoscopic scale, where mutual interactions between biological units and their environment generate emergent phenomena and biological complexity.<sup>4</sup>

### **1.2.3 Complex Systems in Biology:**

The defining characteristics of a complex system include: 1) balance between order and disorder, 2) far-from-equilibrium driven non-linear dynamics, 3) emergence of collective behaviors, 4) embedded information, and 5) historical dependency, where present behavior is partly shaped by the past.<sup>11</sup>

Understanding biological systems' informational content requires prior knowledge of discrete states. However, there is no straightforward correspondence between genetic information and biological functions. Empirical studies show little correlation between genomic and morphological complexity,<sup>12</sup> suggesting that biological systems' total complexity cannot be localized solely at the genomic level.

Despite limited natural variability in biological forms, living entities adopt only a subset of possible morphologies. For example, protein folds are fewer than theoretically expected, suggesting different sequences converge to similar folds due to energy minimization.<sup>13</sup> Bizzarri *et al.*<sup>4</sup> proposed that protein folding results from non-linear interactions between amino acid sequences and microenvironmental constraints, generating complex configurations at the mesoscopic scale. Measuring and analyzing shape thus becomes a powerful method for indicating the macrostates of a system and quantifying its complexity, especially in biological systems characterized by structural irregularities. For instance, Fig. 1 schematically illustrates the interconnectedness between cell shape, cell biomechanics, the cytoskeleton, the gene-protein network, and disease states through chemo-biomechanical pathways.<sup>14</sup>

In clinical practice, analyzing cell and tissue morphology is routine in diagnosing diseases such as cancer. These morphological features can be thought of as representations of the phase space of cellular organization or tissue structure/architecture.

## **1.4 Theories of Carcinogenesis:**

### **1.4.1 Somatic Mutation Theory:**

The dominant somatic mutation theory posits that cancer arises from deterministic mutations at the cellular level, specifically from proto-oncogene point mutations resulting in progressive accumulation of further mutations.<sup>15</sup> This model frames tumor progression as a microevolutionary, Darwinian process.<sup>16</sup> However, its fundamental assumption that all biological information is contained in genes and governs cell functions linearly has proven insufficient.<sup>14</sup>

### **1.4.2 Tissue Organization Field Theory:**

Cancer is now recognized as a complex disease where emergent supracellular phenomena, rather than genetic mutations alone, play pivotal roles. Supragenomic strategies offer a broader and more accurate understanding of carcinogenesis.<sup>17</sup> Experimental evidence highlights the crucial importance of tissue interactions<sup>18</sup> and supports the notion that cancer represents an emergent property of supracellular organization.<sup>19</sup>

The Tissue Organization Field Theory (TOFT) addresses these insights,<sup>20</sup> proposing that cancer arises from disruptions in cell-to-cell junctions, morphostatic gradients, and tensional homeostasis between cells and surrounding stroma, ultimately representing tissue architecture breakdown. This tissue-based view is also endorsed by the emergent theory of carcinogenesis,<sup>21</sup> emphasizing the importance of mesoscopic observations facilitated by quantitative morphological measures. Beyond these perspectives, biological function is deeply embedded in the three-dimensional organization of cells within tissues, the extracellular matrix, and overall anatomical architecture.

## **1.5 Mathematical Approaches to Biological Complexity:**

### **1.5.1 Traditional Modeling Methods:**

Traditionally, physiologists have modelled complex cellular and tissue behaviors using linear differential equations (LDEs) and non-linear differential equations (NLDEs), describing perturbations such as those observed in electrocardiograms.<sup>22</sup> LDE-based models have successfully explained systems like action potential propagation, blood filtration, and insulin feedback control, forming a foundation for understanding physiological homeostasis and disease-related dynamics. Physiological models bridge molecular events with organ-level functions across intermediate structural levels. Multiscale modeling strategies include: 1) constructing anatomically detailed models incorporating hundreds of structural elements (cells, extracellular matrix, membranes, etc.), or 2) employing probabilistic, fractal, or chaotic measures to empirically investigate system complexity.<sup>23,24</sup>

### **1.5.2 Fractional Calculus Framework:**

As shown in Fig. 2, fractional calculus (FC) offers a powerful mathematical framework, bridging integer-order dynamics with fractional-order models.<sup>25</sup> FC extends spatial and temporal scales over which models are valid, expanding investigable phenomena.<sup>26</sup>

Conventional linear models struggle with biological system complexity, while even non-linear models remain constrained by locality and memorylessness, inadequate for systems governed by long-term memory or non-local effects. FC models incorporate non-local interactions and system memory effects through fractional derivatives in space and time,<sup>27</sup> allowing more unified modeling across multiple scales without arbitrary partitioning. In biological contexts, this ability links to the assumption that fractional derivatives can accurately describe complex tissue structures arising from their inherent fractal nature.

Nevertheless, FC modifies several familiar rules from classical calculus. The standard product rule for derivatives is replaced by more complex generalized expressions depending on the chosen fractional derivative definition (Caputo or Riemann–Liouville), requiring careful mathematical consideration before application.<sup>28</sup>

## **1.6 Research Hypothesis and Paper Structure:**

Studying BC as a multiscale, emergent property of tissue systems within an SB framework, quantifying morphological complexity through Fractal Geometry (FG), and modeling biological dynamics using FC may significantly enhance current breast cancer research approaches. While LDEs and NLDEs have been valuable for modeling tumor dynamics and pharmacokinetics, they are limited in accounting for long-term memory, hereditary effects, or anomalous transport behaviors frequently observed in cancer processes. Agent-based and cellular automaton models offer detailed cell-level resolution but often suffer from computational intractability when scaled to simulate tissue-level organization or real-time drug interactions. FC-based models uniquely incorporate memory and non-locality by design, allowing the system's present state to be influenced by its entire dynamic history. Recent applications<sup>29</sup>, demonstrate that FC enables improved modeling of tumor-immune system interactions, sub-diffusive drug transport, radiotherapy dynamics, and chemo-immunotherapy optimization, often outperforming classical models in both predictive accuracy and biological realism. Variable-order fractional models offer flexibility to adapt to evolving tumor states, enhancing multiscale and temporal modeling fidelity. These advantages position FC as a mathematically and biophysically compelling tool for personalized cancer modeling. Although the mathematical foundation of FC is beyond the scope of this review, interested readers are directed to references for accessible introductions to its concepts and applications.<sup>26,30–37</sup>

This review is structured as follows: Section 1 introduces the topic; Section 2 provides a concise overview of fractal geometry, encompassing both mono- and multi-fractal parameters

and analysis; Section 3 examines applications of fractal geometry and fractional calculus in BC research across various contexts within the SB perspective; Section 4 discusses future directions and key challenges; and Section 5 presents concluding remarks.

## 2. Fractal Geometry:

Classical Euclidean geometry has traditionally been used to study the morphology of objects. However, it effectively describes only regular shapes with integer dimensions of one, two, or three, making it insufficient for characterizing the complex and irregular forms often found in natural systems, including cancerous tumors. The irregularity of components such as cells and tissues in tumors highlights the limitations of Euclidean approaches.

Benoît Mandelbrot addressed these limitations by introducing FG, a mathematical framework designed to quantify the morphology of complex, irregular objects. The term *fractal*, derived from the Latin *frāctus*, meaning broken or fragmented, captures the essence of these structures. In general, fractal objects exhibit self-similarity and possess a Hausdorff-Besicovitch dimension greater than their topological dimension. However, exceptions like space-filling curves (e.g., Hilbert curve, Peano curve, Koch curve) show equal fractal and topological dimensions. A comprehensive overview of such curves is available in H. Sagan's work.<sup>38</sup>

An object or pattern is classified as fractal if it displays any of the following types of self-similarity (Fig. 3):

- 1) Exact self-similarity – The object maintains an identical structure or pattern across all scales (Fig. 3(a)).
- 2) Quasi self-similarity – Approximate repetitions of the overall pattern are observed at various scales, albeit with distortions (Fig. 3(b)).
- 3) Statistical self-similarity – Patterns repeat across scales, but only statistically, maintaining scale-invariant statistical properties (Fig. 3(c)).
- 4) Multi-fractals – More than one scaling rule or fractal dimension is present across different regions (Fig. 3(d)).

Another distinctive feature of fractal objects is that their measured properties, such as length, area, or volume, vary depending on the scale of measurement. This is well illustrated by the example of measuring the British coastline, where the measured length increases as the



measurement scale becomes finer. Thus, fractal structures do not have a fixed metric; their measurements are scale-dependent.

The fractal dimension (FD) captures this scaling behavior, relating the measured property to the scale of observation. In spatial data, FD reflects the morphological complexity and degree of roughness, whereas in time series, it describes how fluctuations increase the complexity of the curve, causing it to occupy more of the two-dimensional plane. A higher FD implies greater complexity and long-range fluctuations, while a lower FD suggests smoother, less complex structures.<sup>39</sup> This relationship ties to the Hurst exponent ( $\alpha$ ): values of  $\alpha$  less than 0.5 indicate anti-persistence (negative correlation), while values greater than 0.5 indicate persistence (positive correlation).<sup>40,41</sup> An  $\alpha$  of 0.5 represents complete randomness or Brownian motion-like behavior (Fig. 3(c)).

Various methods have been developed for computing FD, including the Box-Counting Algorithm, Higuchi's Algorithm, and Power Spectrum Density analysis. However, FD alone is often insufficient to fully characterize morphological or textural complexity.<sup>42,43</sup> In this consideration, implementation of the FD measure should be carried out alongside other parameters and not in isolation. One extensively utilized parameter in this context is the fractal's Lacunarity (LC). It is a geometric measure that is applied to investigate the texture-induced morphological complexity or how a complex object/pattern fills the space via investigation of voids/gaps distribution and size.<sup>44</sup> In addition, this parameter has also been described as a measure of rotational or translational invariance, which can describe both fractal and non-fractal (Euclidean) objects/patterns.<sup>45,46</sup> Here, a high (or low) LC, if interpreted for multiple scales, or lacunarity coefficient, if interpreted for a single scale, implies more (or less) rotationally variant objects/patterns with high (or low) spatial heterogeneity. Interestingly, the box-counting method is also used to compute the LC; however, in place of counting the number of boxes required to cover the shape, the change in number of pixels occupied per box at different scales (pixel density) is measured. We provided brief information on the computation of (1) FD using the box-counting algorithm, Higuchi's algorithm, and Power Spectrum Density, and (2) LC using the gliding-box counting algorithm in the following sub-section.

However, it should be noted that investigation using the above-mentioned parameters (FD and LC) implies the assumption of the presence of a single-scaling law in the investigated object's patterns; thus, they can also be called mono-fractal parameters. Nonetheless, fractal objects/patterns can also exhibit multi-fractal self-similar behaviour, which indicates the

presence of more than one scaling parameter (e.g., FD) across scales. Thus, it is recommended to apply multi-fractal analysis along with the routinely utilized mono-fractal studies to avoid ambiguity in results. In this context, the method of Multifractal Analysis has been utilized to investigate the multi-fractal signatures in morphological complexity in a diverse range of systems, including cancer.<sup>47–49</sup> Motivatingly, we have discussed the Two-Dimensional Multifractal Detrended Fluctuation Analysis (2D-MFDFA)<sup>41,47</sup> for extracting multi-fractal parameters and spectrum, respectively, from time series data.

## 2.1 Box-Counting Algorithm:

In general, this method is equivalent to partitioning space into  $n$ -dimensional boxes of defined side length. In other words, the approach utilized measures the characteristic/feature of objects/systems at different scales, plots a graph between feature versus scale, and fits a least-squares regression line where the slope gives the FD of the object or system. The Box-Counting algorithm, in particular, utilizes a set of boxes with defined side length ( $\epsilon$ ), which are then used to make a grid and placed over the object of interest. Subsequently, the number of boxes required to completely cover the object ( $N_\epsilon$ ) is counted. The process is repeated with boxes of different sizes, and a graph is plotted in log-log scale between  $N_\epsilon$  and  $1/\epsilon$  to compute the fractal dimension (Fig. 4(a) and 4(b)).

## 2.2 Higuchi's Algorithm:

The algorithm was first utilized to compute the FD of an irregular time series in the time domain itself.<sup>50</sup> Here, a discrete series of data points is constructed with  $N$  total data points consisting of values at regular intervals. Then, from the single series of data points, new  $k$  sub-sequences  $S_m(k)$  is constructed (Eqn. 1) where,  $m = 1, 2, \dots, d$  represents the initial time, and  $k$  is the time interval with the property  $1 \leq k_{\max} \leq [N/2]$ .<sup>41</sup>

$$S_m(k) : x(m), x(m + d), x(m + 2d), \dots \dots x\left(m + \left\lceil \frac{N-m}{k} \right\rceil k\right) \quad (1)$$

Subsequently, the length  $L_m(k)$  is computed using Eqn. (2),

$$L_m(k) = \frac{1}{k} \left\{ \left( \sum_{i=1}^{\left\lceil \frac{N-m}{k} \right\rceil} |x(m + ik) - x(m + (i-1)k)| \right)^{\frac{N-1}{\left\lceil \frac{N-m}{k} \right\rceil k}} \right\} \quad (2)$$

Here,  $m$  and  $k$  are integers,  $\lceil \cdot \rceil$  and  $\lfloor \cdot \rfloor$  are ceiling and floor function, respectively. The length  $L_m(k)$  represents the normalized sums of the absolute value of the difference in pairs of data points situated at  $k$  distances with initial point/time  $m$ .

For each sub-sequence  $k$ , the mean length is calculated using Eqn. (3),

$$L(k) = \frac{1}{k} \sum_{m=1}^k L_m(k) \quad (3)$$

Finally, the fractal dimension is computed from the least-squares fit of the plot between  $L(k)$  and  $k$  on a double logarithmic scale. It is to be noted that the FD computed from Higuchi's algorithm always lies in the closed interval  $[1, 2]$  where smooth curves like sine and cosine display  $FD = 1$ , while randomly distributed curves will show  $FD = 2$ . Nonetheless, there exists an exception in the case where all the data points possess equal value subsequently,  $L_m(k)$  becomes zero, resulting in  $FD = 0$ .<sup>51</sup>

### 2.3 Power Spectrum Density:

It is based on converting the investigated image to the frequency domain, where the object's/system's features are described by wave numbers using the Fourier transform. In this regard, the power spectrum density (PSD) method brings to light the wavelengths contributing to the investigated feature. Mathematically, this method is the Fourier transform of the autocorrelation function of signals composing the object and identifies the present spatial frequencies within a range of wave-vectors.<sup>52</sup> In image analysis, the power spectrum is given by Eqn. (4),

$$P(k_x, k_y) = c|\vec{k}|^{-\beta} \quad (4)$$

The least square approximation (Eqn. 5) gives the scaling exponent by,

$$\beta = \frac{N \sum_{ij} \log_e |k_{ij}| \log_e P_{ij} - \sum_{ij} \log_e |k_{ij}| \sum_{ij} \log_e P_{ij}}{N \sum_{ij} (\log_e |k_{ij}|)^2 - (\sum_{ij} \log_e |k_{ij}|)^2} \quad (5)$$

Here,  $k$ ,  $N$ ,  $i$ , and  $j$  represents the wave-vectors, number of data points, indices in the horizontal and vertical directions, respectively. Subsequently, the FD is computed using Eqn. (6)<sup>51</sup>,

$$FD = \frac{8-\beta}{2} \quad (6)$$

### 2.4 Gliding Box-Counting Algorithm:

The pictorial representation of the difference between box-counting and gliding box-counting methods is shown in Fig. 4(c). In this approach, the object's image(s) are converted into binary format following the condition in Eqn. (7),

$$g(x, y) = \begin{cases} 1 & \text{if } k(x, y) \geq h^* \\ 0 & \text{otherwise} \end{cases} \quad (7)$$

Here,  $k(x, y)$  signifies an individual object's feature with  $x$  and  $y$  pixel's coordinates and  $h^*$  is the threshold value.

The distribution of lacunar pixels in the object image is evaluated using the gliding-box algorithm. In this method, the number of boxes with length  $l$  and  $p$  lacunar pixels is represented by the frequency distribution  $n(p, r)$ . The probability distribution is computed from Eqn. (8),

$$P(p, r) = \frac{n(p, r)}{(\Delta_a - r + 1) \cdot (\Delta_b - r + 1)} \quad (8)$$

Here, the quantity  $(\Delta_a - r + 1) \cdot (\Delta_b - r + 1)$  is the total number of boxes corresponding to the image's height and base, respectively.

Subsequently, using Eqn. (9), the lacunarity is computed.

$$LC(p, r) = \frac{\sum p^2 \cdot P(p, r)}{[\sum p \cdot P(p, r)]^2} \quad (9)$$

Finally, the LC at each scale is computed from the curve fitting of the decrement in lacunarity with the increment in separation between the pixels ( $r$ ) in the log-log scale.<sup>53</sup>

## 2.5 Multifractal Detrended Fluctuation Analysis:

In this method, the overall fluctuations in a system for the  $q^{th}$  order are given using Eqn. (10),

$$F_q(n) = \left( \frac{1}{M_n N_n} \sum_{k_1=1}^{M_n} \sum_{k_2=1}^{N_n} (F(k_1, k_2, n))^q \right)^{1/q} \quad (10)$$

Here, the moment ( $q$ ) can take any integer value,  $M_n \times N_n$  represents the disjoint segments of the feature with equal sizes  $n \times n$ . The least squares fit of the graph between  $F_q(n)$  and  $q$  in log-log scale gives the scaling of the fluctuation function, known as the Generalized Hurst exponent  $h(q)$ . The mass exponent is computed from  $h(q)$  using Eqn. (11),

$$\tau(q) = qh(q) - FD \quad (11)$$

In Eqn. (11), FD represents the fractal dimension of the geometric support of the multifractal measure. In addition, it is noteworthy that the parameters  $h(q)$  and  $\tau(q)$  displays a non-linear behaviour in the case of the presence of multifractal characteristics in a system.

In two-dimensional MFDFA, the embedding space is partitioned into  $N(\varepsilon)$  boxes of a size  $\varepsilon$ . The partition function is defined from Eqn. (12) as,

$$Z(q, \varepsilon) = \sum_{i=1}^{N(\varepsilon)} (p_i)^q \quad (12)$$

Assuming  $p_i \sim \varepsilon^\alpha$  in the limit  $\varepsilon \rightarrow 0$ , the number of boxes with a scaling exponent between  $\alpha$  and  $\alpha + d\alpha$  is nearly equivalent to  $\varepsilon^{-f(\alpha)d\alpha}$ . Thus, Eqn. (12) modifies into

$$Z(q, \varepsilon) = \int \varepsilon^{-f(\alpha)+\alpha q} d\alpha \quad (13)$$

The smallest value of  $\varepsilon^{-f(\alpha)+\alpha q}$  satisfies Eqn. (14) given as,

$$\frac{d}{d\alpha}[\alpha q - f(\alpha)]_{\alpha_m} = 0 \quad (14)$$

$$\Rightarrow f'(\alpha_m) = q \text{ and } Z(q, \varepsilon) = \varepsilon^{\tau(q)}$$

$$\text{Thus, } \frac{d\tau}{dq} = \alpha_m + \frac{d\alpha_m}{dq} q - f'(\alpha_m) \frac{d\alpha_m}{dq} = \alpha_m$$

$$\Rightarrow f(\alpha_m) = q \frac{d\tau}{dq} - \tau \quad (15)$$

The continuous curve traced by  $f(\alpha_m)$  with  $\alpha_m$  with a variation of  $q$  in the interval  $[-\infty, \infty]$  is known as the multifractal spectrum (Fig. 4(d)).<sup>41,54</sup> In the framework of multifractal analysis,  $\alpha(q)$  and  $f(\alpha)$  are known as the Holder exponent and singularity spectrum, and measure the local singularity or discontinuity in the function and global singularity, respectively. In addition, the difference between the maximum and minimum value of the Holder exponent or global singularity (Hausdorff fractal dimension) determines the strength of multifractality.<sup>41,55</sup>

### 3. Applications of FG and FC in BC research: An SB Perspective

A crucial predictor of BC prognosis is the status of axillary lymph nodes. However, its role in guiding systemic adjuvant chemotherapy remains unclear, as reported in various studies.<sup>56–59</sup> Rizki and Bissell<sup>60</sup> observed that malignant neoplasms, such as invasive BC, often lack structural organization and functional coordination with surrounding normal tissues. They argued that this irregularity leads to an increase in morphological complexity at the subcellular, cellular, and multicellular levels, and quantifying this complexity could correlate with patient outcomes. In this context, Tambasco *et al.*<sup>61</sup> computed the fractal dimension (FD) of segmented histological structures from pan-cytokeratin-stained breast tissue microarrays using a box-counting algorithm. Analyzing samples from 379 patients, they demonstrated that increased epithelial morphological complexity strongly and significantly correlated ( $p < 0.001$ ) with disease-specific and overall survival. Here, epithelial morphological complexity was defined as the scale-invariant irregularity of epithelial architecture, captured quantitatively by FD, as it reflects disorganization at sub-cellular (keratin distribution and nuclear shape), cellular (cell contours), and multicellular (glandular formation) levels.

Another key feature distinguishing malignant tumors from normal tissues is uncontrolled growth, requiring extensive vascularization. This emphasizes the critical role of angiogenesis in tumor progression.<sup>62</sup> Studies have reported significant contributions of non-cancerous cells in angiogenesis, metastasis, and cell proliferation. This implies that cancer tumours can be regarded as complex tissues with alterations in the original tissue homeostasis, and where non-cancerous cells are chosen to function according to the new tissue dynamics dictated by the

cancerous cells.<sup>63</sup> This observation is in agreement with Principle 10 in the theory of the emergence of carcinogenesis, which proposes that cancer represents the formation of a new tissue-level system arising from the components of the original tissue but reorganized around a new purpose, i.e., unconstrained growth. In this emergent system, non-cancerous cells such as endothelial, stromal, and immune cells are co-opted or reprogrammed to function following the tumor's altered dynamics and support its progression.<sup>21</sup>

It has also been argued that intense vascularization is an essential condition for neoplastic development.<sup>64</sup> In this regard, the growth of solid neoplasm was proposed to accompany neovascularization, where the growth of new capillaries is more vigorous and continuous than the growth of capillary shoots in fresh wounds and inflammations.<sup>65</sup> A major feature in neovascularization is the growth factor, namely, endothelial cells, in tumour blood, which responds to angiogenic factors by upregulating the proliferation, migration, and differentiation rates while lowering the apoptosis rate. However, these effects are reported to be insufficient in explaining the vascular architecture in tumours. Also, in the absence of growth factor, as a consequence of the oxygen gradient in normal tissues, the tumour vasculature grows vigorously through a heterogeneous extracellular matrix by the process of invasion percolation.

Baish and Jain<sup>66</sup> used a computer model of tumour vasculature based on the process of percolation to investigate the transport of drugs and oxygen to tumours. They observed a lack of overall network optimization in tumour tissues when compared to normal tissues. Specifically, they noted that regressing of tumour e.g., androgen-dependent Shionogi modelled blood vessels after hormone removal display a notable fractal scaling (possibly, space-filling behaviour) similar to normal tissues which indicates that reduction in number of vessels and consequently, vessel density may improve the transport of blood-borne substances to the tumour which can thrive tumour growth. Similar results were reported for flow correlated percolation during remodelling of vessels in growing solid tumours.<sup>67</sup> Accordingly, an emphasis should be given to the need for tumour investigation from an architectural and physiological perspective to aid in molecular diagnostic tools.

These reported observation of simultaneous progression in neovascularization with metastasis along with the association of periductal neovascularization with tumour size and microcalcification in Ductal Carcinoma *in situ* (DCIS) of the breast<sup>68</sup> demands the need of novel techniques for investigating the physiological/architectural effect of tumour size, vascularity, and detection of microcalcification which can aid to assess the functioning of drugs against neovascularization subsequently, preventing development of invasive BC. In this regard, the prognostic value of BC tumours was assessed using FD and lacunarity parameters

on a group of 40 low-risk patients who did not undergo any systematic treatment.<sup>69</sup> The samples were collected from surgically removed tissue sections and were subsequently stained with Hematoxylin and Eosin dyes. The FD and LC were computed from the digitally photographed tissue sections (x400 magnification) using the box-counting algorithm. They observed, via comprehensive statistical evaluation, a correlation between FD and lacunarity with tumours' biological properties, thus offering a promising strategy for assessing the risk of distant metastasis independently of molecular biomarkers economically. In addition, they reported the fractal characteristics of native tumour histology as effective prognostic markers with a long median follow-up period of 5 months.

Ribeiro *et al.*<sup>70</sup> inspected the form and growth process of avascular tumours, considering the competition between cells. The proposed model reproduced the conventionally observed early-stage exponential growth followed by power-law growth resulting from the tumour's fractal structure, facilitated by the emergent optimal value of FD as a consequence of interaction between cells. In addition, a similar relation was observed to hold between the intrinsic replication-competition rate between cells and the allocation of energy in growing animals. In other words, a universal behaviour was proposed to exist in the growth of avascular tumours and animals, which can be modelled using the Bertalanffy-Richards model. Stimulatingly, a breast cancer competition model was modelled considering the population dynamics among healthy, cancer stem, and tumour cells, respectively, along with the effect of excess estrogen and the body's natural immune response on the cell populations using Liouville-Caputo and Caputo-Fabrizio-Caputo fractional derivatives. An iterative (numerical) scheme was employed using the Laplace transform (Atangana-Toufik) to obtain the special numerical solutions. The results suggested the positive significance of fractional derivatives for revealing the complexity of dynamics in the proposed model.<sup>71</sup> In a different work, d'Onofrio extended the mean-field theory proposed by Mombach *et al.*<sup>72</sup>, which aimed to mechanistically link macroscopic tumour properties to the microscopic cell properties, via focusing on the role of cell-cell interactions only. He concluded that the interaction of a cell with the microenvironment can be encoded in the form of noise-induced fluctuations from considering the parameters that take into account the proliferation rate of a cell resulting from its baseline replication rate and a constant related to the effectiveness of inhibitory actions. Interestingly, these two parameters were integrated in a single equation by assuming a fractal spatial structure of cell populations.<sup>73</sup> This observation indicates that quantification of morphological complexity in cell clusters, representing the spatial organization of cells, can provide useful diagnostic information.

Yokoyama *et al.*<sup>74</sup> studied the implication of irregularity in cell cluster edge-shape in cytological diagnosis of BC using image analysis. They investigated the edge-shape irregularity in cell clusters as a diagnostic criterion for differentiating between benign and malignant tumours via comparison of breast tumours demonstrating weak cellular atypia in low-grade invasive ductal carcinoma (IDC) using box-counting computed FD along with 8 other parameters. Fine needle aspiration specimens of tumours were collected from 37 patients (16 low-grade IDC and 21 benign fibroadenoma (FA)), and 740 cell clusters were examined based on grouping into three types, viz., IDC clusters, FA with irregular clusters, and FA with regular clusters. Interestingly, they reported the average cluster size area in FA with irregular clusters to be approximately 3 times larger than that of IDC clusters. Consequently, they emphasized the focus on irregularities of cluster edge-shape in the case of differentiating between IDC and FA for accurate diagnosis.

In a similar consideration to cells, the effectiveness of FD, computed using fractional Brownian motion, was assessed to differentiate between normal and cancerous cells from the assumption that the cell nucleus displays a fractal property.<sup>75</sup> The results suggested the significance of scaling range in fractal investigation since the range of scale over which cancerous cells displayed fractal properties was considerably larger than normal cells.

In the context of microcalcification, a hierarchical interaction between morphological descriptors and parenchyma FD (box-counting algorithm) was studied for discriminating benign and malignant categories using digital mammography.<sup>76</sup> The study included 31 patients with microcalcification detected from mammography and confirmed from stereotactic biopsies, and were classified according to the Breast Imaging-Reporting and Data System (BI-RADS) along with parenchyma FD and biopsy size. The results implied the possible usage of quantitative shape evaluation and parenchyma FD for promising prediction of BI-RADS score. In addition, the lesions' area and parenchyma FD exhibited a complex distribution for malignant breast MC, which was in agreement with the observed qualitative morphological patterns.

In image analysis, the point at which brightness changes sharply or has discontinuity indicates edges. The detection of edges decreases the amount of data to be processed and filters redundant information while preserving the structural information. Stimulatingly, fractional derivatives or operators were proposed for improving the edge-detection and consequently, contrast and texture of mammograms for easy detection of microcalcifications.<sup>77</sup>

It is also noteworthy that distortion of architecture in breast parenchyma, including radiation of spiculation from a point and focal distortion at the parenchyma edge without increase in



breast mass density, is the third most common indication observed in the mammographic signature of nonpalpable BC.<sup>78</sup> This architectural distortion can appear in the initial stages of BC; however, owing to its ability to mimic normal breast tissues, its presence is often missed during screening and is reported to be one of the most common factors in false-negative cases.<sup>79</sup> In regards to the aforementioned, Banik *et al.*<sup>80</sup> aimed to develop a computer-aided diagnostic technique for the detection of architectural distortion in prior mammograms of interval-cancer cases utilizing Gabor filters, linear phase portrait analysis, FD from Power Spectrum Density, and the angular spread of power in the frequency domain. They utilized 1745 digitized mammograms of 170 patients obtained from the Alberta Program for the Early Detection of BC. Prior mammograms of interval-cancer cases (106) were identified by a radiologist, and subsequently, two categories, viz., visible architectural distortion (38) and questionable/invisible architectural distortion (38) were made for the study. The outcome suggested that a combination of FD and angular spread of power can be used to detect the subtle signatures of architectural distortion in mammograms. Another study, although carried out on a small set of 19 mammograms, reported the combination of FD and lacunarity, giving a prediction accuracy of 90% in the detection of architectural distortion.<sup>81</sup> Furthermore, a hybrid feature extraction method from mammograms to detect and classify microcalcification, architectural distortion, breast masses (or, space-occupying lesions), and bilateral symmetry (or, asymmetry of breast parenchyma between two sides) was proposed based on multifractal analysis (Renyi FD spectra), directional and morphological analysis, and Gabor filters. Here, the regions of interest were identified using intuitionistic fuzzy clustering, and feature classification was done using a self-adaptive resource allocation network. The proposed method was implemented on images taken from open-access databases- Digital Database for Screening Mammography (DDSM) and Mammographic Image Analysis Society (MIAS) and subsequently, exhibited accuracy (sensitivity) of 93.75% (0.93) and 94.72% (0.92) for DDSM and MIAS, respectively.<sup>82</sup>

Nonetheless, detection of masses is challenging since normal and abnormal (pre-cancerous/cancerous) tissues look similar, which escalates the emergence of false positives in computer-aided diagnostics. To overcome this limitation, mammograms facilitated five feature extraction methods were proposed, out of which two are Hilbert space-filling curve-based image representation and fractal texture analysis.<sup>83</sup> They argued that the extraction of features directly from the complete regions of interest overcomes the need for image segmentation and also takes into account lesions surrounding the tissues, which can be useful in BC diagnosis. Another study utilized Hilbert curves to investigate a set of 111 mass contours for

differentiating between 65 benign and 46 malignant masses. An accuracy of 99% was achieved in terms of the area under the receiver operating characteristic (ROC) curve.<sup>84</sup> The possible effective investigation of one-dimensional contours in BC diagnosis can overcome the computationally complex analysis of two-dimensional images. In this context, the two-dimensional tumour images were converted into their one-dimensional sequences or contour signatures, and subsequently, the FD of breast masses was computed using Higuchi's algorithm. The authors suggested the method to be easy and quick in implementation, and can serve as an auxiliary measure in pathological diagnosis.<sup>85</sup>

In another work, although using Higuchi's algorithm, ultrasound-radio frequency time-series analysis was performed to classify malignant breast lesions. A machine learning framework combined with time-series features was used to generate malignancy maps for depicting the likelihood of malignancy within a region of 1 mm<sup>2</sup> containing suspicious lesions. The resulting ROC curve exhibited an accuracy of 86% (81%) at a 95% confidence interval from Support Vector Machines (Random Forest Classification) in combination with time-series features, and consequently, can reduce the number of unnecessary biopsies in mammography screening<sup>86</sup> for the early detection of BC.

#### **4. Future Prospects and Challenges:**

We have outlined and discussed from the perspective of SB the prospective application of fractal geometry and fractional calculus in the investigation of breast cancer in various contexts via quantification of cells (microscopic), tissues (mesoscopic), and even tumours (macroscopic) morphological complexities and dynamics.

A notable characteristic of FG, which can be of great importance, is its possible usage in phenotype determination in case of limited samples. This is highlighted from the work of Ferro *et al.*,<sup>87</sup> which reported the calculation of the mean FD of nuclear chromatin using the box-counting algorithm from only 30-40 cells and showed the significance of FD in the prediction of patients' survival suffering from multiple myeloma. This observation can be of significant interest in the case of positive/negative BC having a limited number of samples, such as in fine needle aspiration.

It is worth noting that most of the discussion in the previous section is concerned with mono-fractal analysis of images in two-dimensions, a few efforts with one-dimensional analysis, and almost negligible advances in three-dimensions. In addition, multi-fractal analysis has been reported to display the scaling of the FD parameter only. Furthermore, dynamic contrast enhanced magnetic resonance imaging is a robust technique for the diagnosis of BC in high-

risk women, although similar contrast between benign masses and malignant lesions limits the sensitivity of the technique. Regarding the previously mentioned, Soares *et al.*<sup>88</sup> proposed a three-dimensional multifractal analysis with lacunarity as the multifractal measure. The result suggested the effectiveness of the method in differentiating between benign and malignant samples as judged by the support vector machine classification method, with an accuracy of 96%.

Furthermore, false positive detection of masses and microcalcification in computer-aided diagnosis, induced by the need for image segmentation, is a limitation in the most economic screening of BC, i.e., via mammography. In the context of the previously reported observation, this can be overcome through the utilization of space-filling curves and fractional derivatives.

The significance of neovascularization has also been discussed in the previous section and has been reported to be an important prognostic factor in BC, considering vascular density.<sup>89</sup> Contrastingly, morphometric parameters, i.e., vascular FD and total vascular area associated with vessel shape and size, respectively, in tissue specimens (48 carcinoma and 17 benign) extracted from 17 randomly selected oral squamous cell carcinoma patients were assessed. The statistical analysis exhibited the importance of vascular FD in the detection of angiogenesis.<sup>90</sup>

According to Dhabi *et al.*<sup>83</sup> BC arises from the cells and develops locally before metastasizing to the lymph nodes and internal organs. This observation could indicate towards significance of cell-cell interaction or competition in facilitating BC growth thus, investigating the dynamics of interaction between cells using fractional calculus via the usage of various kernels can enable us to understand the complex dynamics of the cellular system.

The Epithelial-to-Mesenchymal transition (EMT) is generally associated with a decrease in cell adhesion, loss of contact between cells, and induction of morphological fluctuations. In addition, this transition is responsible for the development and progression of tumours and, consequently, metastasis. The influence of cytokine transforming growth factor- $\beta$ 1 (TGF- $\beta$ 1) induced EMT on structure, migration, cytoskeletal dynamics, and long-term correlations in selected mammalian cell lines was studied utilizing time-resolved impedance analysis.<sup>91</sup> In particular, fluctuations in impedance time series, which can be interpreted as structural and/or adhesive alteration of cells, were examined using detrended fluctuation analysis. Consequently, the authors reported insights into the phenotype state and metastatic potential of the investigated cell lines.

The sigmoidal Gompertzian curves are conventionally utilized in modelling the growth of malignant tumours. According to Waliszewski and Konarski<sup>92</sup> the normalized Gompertzian curve can be fitted with a power function where the exponent denotes the temporal FD. They

claimed that not only the space occupied by interacting cells but also the intrasystemic time for tumour growth possesses a fractal structure characterized by the exponent in the power function and tends towards Euclidean dimension with tumour progression.

FD has also been implemented to quantify the structural complexities of the external nuclear membrane envelope and membrane-bound heterochromatin domains of Michigan Cancer Foundation-7 (MCF-7) human BC cells, triggered by steroid hormones like  $17\beta$ -estradiol or dexamethasone, at the initiation stage of growth. Subsequently, it was observed that 1 nM concentration of  $17\beta$ -estradiol noticeably augmented the structural/morphological complexities or the unfolding of DNA in membrane-bound heterochromatin domains, while the same dosage of dexamethasone reduced the irregularities after 5 minutes of treatment, as inferred from the FD values.<sup>93</sup>

Although in SB, cancer investigation should be concerned with cells, tissues, and tumours, cancer is also identified as a genetic disease where tumours are caused by a sequence of genetic abnormalities, causing the cells to be either normal or tumour-generating; thus, understanding the sequence is of primary importance in understanding carcinogenesis. In this regard, we investigated the geometrically ordered and disordered states of nucleotide spatial distribution in mutation-facilitated oncogenes, corresponding to different cancers, including BC. Subsequently, we identified distinct fusion mutation-facilitated geometric states in distinct cancer types.<sup>94</sup> In another unrelated study, an oncogenetic tree model for oncogenesis was proposed by Desper *et al.*<sup>95</sup> from comparative genome hybridization data. Here, the root represents the state of a normal cell or state of a tissue with no somatic mutations, leaves represent recurrent genomic alterations, inner nodes signify hidden events, and subtrees represent tumours. As per the model, the alterations are irreversible, and cancerous cells are identified from the presence of changes in all four tree parts. This provided a path model for tumour progression in which the cell started from a normal and healthy state and proceeded down the path with four vertices representing different genetic alterations. According to the authors, “genetic changes will not always occur in the order of the path, but the path defines the preferred order,” and the tree can be formally modelled through *p-adic* (*p* stands for *prime numbers*) analysis methods.<sup>96</sup> Interestingly, *p-adic* calculus has been argued to apply to fractal analysis.<sup>97</sup> Additionally, the *p-adic* number system offers a possible approach for the representation of hierarchically organized complex networks where constructing an enormous space of hierarchical structures is equivalent to combining sequences of numbers. Hua and Hovestadt<sup>98</sup> demonstrated the fitting of the size of the few largest components in hierarchical structures to empirical data, where the utilization of *p-adic* enables the Erdős–Rényi model to

simulate genetic interaction networks. In another work, a *p-adic* model of DNA sequence and genetic code was proposed by Dragovich and Dragovich.<sup>99</sup> The basic elements, i.e., nucleotides, codons, and genes, comprise the ultrametric *p-adic* information space in their model. Subsequently, they observed the 5-adic model to be appropriate for DNA sequence, and its combination with 2-adic distance is suitable for genetic code, where the *p-adic* distance between codons is related to the degeneracy of the genetic code.

Moreover, another measure of mono-fractals, succolarity, has recently been prominently utilized in the analysis of textures in different systems.<sup>100,101</sup>, although it has found limited usage in biology as of now. It is considered a measure of the degree of percolation/connectivity/intercommunication/anisotropy. Cattani and Pierro<sup>102</sup> investigated the utilization of FD, LC, Shannon entropy, complexity, and succolarity in the classification of DNA sequences from the nucleotide distribution. The study was performed on the genome of *Drosophila melanogaster* with a special focus on the chromosome 3r using binary images of the indicator matrix. A negative correlation between FD and Shannon entropy with succolarity was reported, indicating that the value of succolarity near zero (one) signifies minimum (maximum) structural and informational complexity, respectively. Interestingly, succolarity has been utilized in the classification of breast cancer masses collected from the MIAS and INbreast datasets. According to the authors, this parameter is a measure of the roughness of the contours and, in combination with FD and lacunarity, can effectively differentiate between normal, benign, and malignant tumours. However, no clear correlation between FD and succolarity was observed in this study.<sup>103</sup> We introduced a modified direction-independent measure, namely the succolarity reservoir, to account for latent-connectivity in tissue architecture from mammograms.<sup>104</sup> The measure was observed to hold statistical significance, in addition to FD and multifractality strength, for differentiating between normal and malignant categories. In addition, it also exhibited the potential to correlate breast texture to BC molecular subtypes.

From the aforementioned, it can be speculated that FG can play a pivotal central role in the investigation of BC, from the standpoint of SB, in various prospects, i.e., from early diagnosis, effect of dosage or treatment, metastasis, to prognosis. In addition, its analytical treatments and combination with other frameworks like fractional calculus and number theory (*p-adic*) can provide invaluable insights from the scale of tumours to genes.

Nevertheless, it can also be realized that there is a lack of standardized protocols in the application of FG to BC research. In the context of image analysis, input parameters like selection accuracy of regions of interest, resolution, bit depth, and signal-to-noise ratio can

affect the outcome from fractal analysis. In addition, the analyses are almost always performed with two-dimensional binary images, which can enable loss of information during the binarization process.<sup>105</sup> These necessities a need for the development of tools capable of analysing binary, grey-scale, and colour images in one-, two-, and three-dimensions, which can contribute to enhancement in sensitivity and selectivity of the analysis. In addition, in particular to histological specimens, sample processing can introduce subtle artifacts thus, attempts should be made to conserve the cellular and tissue morphology to have meaningful results from the utilization of FG and its combination with FC.

## **5. Conclusions:**

Classical Euclidean geometry is insufficient to describe the irregular and complex morphologies commonly observed in biological systems. To address this, fractal geometry has been employed to investigate morphological complexities and irregularities across a wide range of biological structures. It is also well-established that the structure and function of individual cells and tissues fundamentally determine the complexity of living systems. Thus, it can be inferred that the function of biological entities is closely linked to the three-dimensional architecture of cells within tissues, the extracellular matrix, and overall anatomical organization. These observations highlight the significant potential of FG in analyzing the complexities of cells, tissues, and even entire organs.

Moreover, fractional derivative models, which incorporate non-locality and system memory effects through fractional-order space and time derivatives, enable the modeling of biological phenomena across multiple spatial and temporal scales without requiring partitioning. This approach is particularly relevant to biological systems, where it is assumed that fractional derivatives can effectively capture complex tissue structures arising from their fractal nature.

Based on these considerations, it can be hypothesized that investigating BC within the framework of SB, through the quantification of morphological complexity in cells, tissues, and tumors across spatial and temporal scales using FG and studying their dynamics with FC, could significantly advance various aspects of BC research.

In this review, we have presented examples demonstrating the potential applications of FG and FC in BC research. We also emphasized that combining fractal geometry with fractional calculus and number theory could provide valuable insights, spanning scales from tumors down to genes. Although this discussion is not an exhaustive exploration of all possibilities, we aim to encourage the wider application of diverse imaging modalities and the development of

methods and tools that integrate FG and FC to overcome existing limitations in BC investigation.

## References:

1. Sung, H., Ferlay, J., Siegel, R. L., Laversanne, M., Soerjomataram, I., Jemal, A., & Bray, F. Global Cancer Statistics 2020: GLOBOCAN Estimates of Incidence and Mortality Worldwide for 36 Cancers in 185 Countries. *CA. Cancer J. Clin.* **71**, 209–249 (2021).
2. Wild, C.P., Weiderpass, E., Stewart, B. W. (Ed.) World Cancer Report: Cancer Research for Cancer Prevention, Lyon France: International Agency for Research on Cancer (2020). <http://publications.iarc.fr/586>
3. Hornberg, J. J., Bruggeman, F. J., Westerhoff, H. V. & Lankelma, J. Cancer: A Systems Biology disease. *BioSystems* **83**, 81–90 (2006).
4. Bizzarri, M., Giuliani, A., Cucina, A., Anselmi, F. D., Soto, A. M., & Sonnenschein, C. Fractal Analysis in a System Biology Approach to Cancer. *Semin Cancer Biol.* **21**, 175–182 (2011).
5. Kitano, H. Systems biology: A brief overview. *Science*. **295**, 1662–1664 (2002).
6. Strohmman, R. C. Organization becomes cause in the matter. *Nat. Biotechnol.* **18**, 575–576 (2000).
7. Laughlin, R. B., Pines, D., Schmalian, J., Stojković, B. P. & Wolynes, P. The middle way. *Proc. Natl. Acad. Sci.* **97**, 32–37 (2000).
8. Hood, L. & Galas, D. The digital code of DNA. *Nature* **421**, 444–448 (2003).
9. Westerhoff, H. V. & Palsson, B. O. The evolution of molecular biology into systems biology. *Nat. Biotechnol.* **22**, 1249–1252 (2004).
10. Noble, D. Claude Bernard, the first systems biologist, and the future of physiology. *Exp. Physiol.* **93**, 16–26 (2008).
11. Nicolis, G., Prigogine, I., & Carruthers, P. Exploring Complexity: An Introduction. *Phys. Today*. **43**, 96–97 (1990).
12. Stent, G. S. Strength and Weakness of the Genetic Approach to the Development of the Nervous System. *Ann. Rev. Neurosci.* **4**, 163–194 (1981).



13. Denton, M. & Marshall, C. Laws of form revisited. *Nature* **410**, 417 (2001)
14. Dinicola, S., D'Anselmi, F., Pasqualato, A., Proietti, S., Lisi, E., Cucina, A., & Bizzarri. A systems biology approach to cancer: Fractals, Attractors, and Nonlinear Dynamics. *Omi. A J. Integr. Biol.* **15**, 93–104 (2011).
15. Hahn, W. C., Counter, C., Lundberg, A., Beijersbergen, R. L., Brooks, M. W. & Weinberg, R. A. Creation of human tumour cells with defined genetic elements. *Nature* **400**, 464–468 (1999).
16. Michor, F., Iwasa, Y. & Nowak, M. A. Dynamics of cancer progression. *Nat. Rev. Cancer* **4**, 197–205 (2004).
17. Folkman, J., Hahnfeltdt, P. & Hlatky, L. Cancer: looking outside the genome. *Nat. Rev. Mol. Cell Biol.* **1**, 76–79 (2000).
18. Olumi, A. F., Grossfeld, G. D., Hayward, S. W., Carroll, P. R., Tlsty, T. D. & Cunha, G. R. Carcinoma-associated Fibroblasts Direct Tumor Progression of Initiated Human Prostatic Epithelium. *Cancer Res* **59**, 5002-5011 (1999).
19. Weaver, V. M. & Gilbert, P. Watch thy neighbor: Cancer is a communal affair. *J. Cell Sci.* **117**, 1287–1290 (2004).
20. Bertolaso, M. The Tissue Organization Field Theory and the Anti-reductionist Campaign. In: *Philosophy of Cancer: History, Philosophy and Theory of the Life Sciences* **18**, Springer, Dordrecht (2016).
21. Sigston, E. A. W. & Williams, B. R. G. An Emergence Framework of Carcinogenesis. *Front. Oncol.* **7**, 1–14 (2017).
22. Keener, J. P. & Sneyd, J. (Ed.) *Mathematical Physiology I: Cellular Physiology*. Springer-Verlag New York 2009 (2008). <https://doi.org/10.1007/978-0-387-75847-3>
23. Bar-Yam, Y. *Dynamics of Complex Systems*. CRC Press (2019) <https://doi.org/10.1201/9780429034961>

24. Shelhamer, M. *Nonlinear Dynamics in Physiology: A State-Space Approach*. *Nonlinear Dynamics in Physiology: A State-space Approach*. World Scientific (2006). <https://doi.org/10.1142/6240>.
25. West, B. J. Bologna, M., & Grigolini. *Physics of Fractal Operators*. Springer New York. (2003). <https://doi.org/10.1007/978-0-387-21746-8>
26. Magin, R. L. Fractional Calculus in Bioengineering. *Crit. Rev. Biomed. Eng.* **32**, 1–104 (2004).
27. Hilfer, R. (Ed.) *Applications of Fractional Calculus in Physics*. World Scientific (2000). <https://doi.org/10.1142/3779>
28. Magin, R. L. Fractional calculus models of complex dynamics in biological tissues. *Comput. Math. with Appl.* **59**, 1586–1593 (2010).
29. Vieira, L. C., Costa, R. S. & Valério, D. An Overview of Mathematical Modelling in Cancer Research: Fractional Calculus as Modelling Tool. *Fractal Fract.* **7**, 1–22 (2023).
30. Lazarević, M. P., Rapačić, M. R., & Šekara, T. B. Introduction to fractional calculus with brief historical background. In book: *Advanced Topics on Applications of Fractional Calculus on Control Problems, System Stability and Modeling*. WSEAS Press (2014).
31. Sun, H. G., Zhang, Y., Baleanu, D., Chen, W. & Chen, Y. Q. A new collection of real world applications of fractional calculus in science and engineering. *Commun. Nonlinear Sci. Numer. Simul.* **64**, 213–231 (2018).
32. West, B. J. Fractal physiology and the fractional calculus: a perspective. *Front. Physiol.* **1**, (2010).
33. Magin, R. L. Fractional Calculus in Bioengineering, Part 2. *Crit. Rev. Biomed. Eng.* **32**, 105–193 (2004).
34. Magin, R. L. & Bourne, J. R. Fractional Calculus in Bioengineering, Part 3. *Crit. Rev. Biomed. Eng.* **32**, 195 (2004).
35. Alinei-Poiana, T., Dulf, E-H. & Kovacs, L. Fractional calculus in mathematical oncology. *Sci. Rep.* **13**, 10083 (2023).

36. West, B. J. The Fractal Tapestry of Life: II Entailment of Fractional Oncology by Physiology Networks. *Front. Netw. Physiol.* **2**, 1–29 (2022).
37. West, B. J. The Fractal Tapestry of Life: III Multifractals Entail the Fractional Calculus. *Fractal Fract.* **6**, 225 (2022).
38. Sagan, H. *Space-Filling Curves*. Springer New York, NY (1994).  
<https://doi.org/10.1007/978-1-4612-0871-6>
39. Eghball, B., Hergert, G. W., Lesoing, G. W. & Ferguson, R. B. Fractal analysis of spatial and temporal variability. *Geoderma* **88**, 349–362 (1999).
40. Das, A., Matos, R. S., Pinto, E. P., Yadav, R. P., Țălu, Ș, & Kumar, S. 3D micromorphology-contact resistance-conductivity insights of quasi 2D Cd<sub>1-x</sub>Pb<sub>x</sub>S thin films: Investigation based on stereometric and fractal analysis. *Mater. Chem. Phys.* **278**, 125635 (2022).
41. Das, A., Jaiswal, J., Yadav, R. P., Mittal, A. K., Țălu, Ș, & Kumar, S. Complex roughening dynamics and wettability mechanism in MoS<sub>2</sub> thin films — A system theoretic approach. *Phys. A Stat. Mech. its Appl.* **624**, 128989 (2023).
42. Mandelbrot, B. B. A Fractal's Lacunarity, and how it can be Tuned and Measured. *Fractals Biol. Med.* 8–21 (1994) doi:10.1007/978-3-0348-8501-0\_2.
43. Landini, G. Fractals in microscopy. *J. Microsc.* **241**, 1–8 (2011).
44. Tolle, C. R., McJunkin, T. R. & Gorsich, D. J. An efficient implementation of the gliding box lacunarity algorithm. *Phys. D Nonlinear Phenom.* **237**, 306–315 (2008).
45. Karperien, A., Ahammer, H. & Jelinek, H. F. Quantitating the subtleties of microglial morphology with fractal analysis. *Front. Cell. Neurosci.* **7**, 1–34 (2013).
46. Smith Jr., T. G., Lange, G. D. & Marks, W. B. Fractal methods and results in cellular morphology - dimensions, lacunarity and multifractals. *J. Neurosci. Methods* **69**, 123–136 (1996).

47. Das, A., Chawla, V., Jaiswal, J., Begum, K., Pinto, E. P., Matos, R. S., Yadav, R. P., Țălu, Ș. & Kumar, S. Fractal dimension of heights facilitates mesoscopic mechanical properties in ternary hard film surfaces. *J. Appl. Phys.* **134**(22), 225302 (2023).
48. Chanu, A. L., Chingangbam, P., Rahman, F., Singh, R. K. B. & Kharb, P. Analysis of the structural complexity of Crab nebula observed at radio and infrared frequencies using a multifractal approach. <https://doi.org/10.48550/arXiv.2206.04717>
49. Huynh, P. K., Nguyen, D., Binder, G., Ambardar, S., Le, T. Q., & Voronine, D. V. Multifractality in Surface Potential for Cancer Diagnosis. *J. Phys. Chem. B* **127**, 6867–6877 (2023).
50. Higuchi, T. Approach to an irregular time series on the basis of the fractal theory. *Phys. D Nonlinear Phenom.* **31**, 277–283 (1988).
51. Ahammer, H. Higuchi Dimension of Digital Images. *PLoS One* **10**, e0119394 (2015).
52. Jacobs, T. D. B., Junge, T. & Pastewka, L. Quantitative characterization of surface topography using spectral analysis. *Surf. Topogr.: Metrol. Prop.* **5**, 013001 (2017).
53. Pinto, E. P., Pires, M. A., Matos, R. S., Zamora, R. R. M., Menezes, R. P., Araújo, R. S. & de Souza, T. M. Lacunarity exponent and Moran index: A complementary methodology to analyze AFM images and its application to chitosan films. *Phys. A Stat. Mech. its Appl.* **581**, 126192 (2021).
54. Yadav, R. P., Singh, U. B., Mittal, A. K. & Dwivedi, S. Investigating the nanostructured gold thin films using the multifractal analysis. *Appl. Phys. A* **117**, 2159–2166 (2014).
55. Sahoo, G. R., Dey, R., Das, N., Ghosh, N. & Pradhan, A. Two dimensional multifractal detrended fluctuation analysis of low coherence images for diagnosis of cervical precancer. *Biomed. Phys. Eng. Express* **6**, 025011 (2020).
56. Mirza, A. N., Mirza, N. Q., Vlastos, G. & Singletary, E. S. Prognostic Factors in NodeNegative Breast Cancer: A Review of Studies With Sample Size More Than 200 and Follow-Up More Than 5 Years. *Ann. Surg.* **235**, 10–26 (2002).
57. Elledge, R. M. & McGuire, W. L. Prognostic factors and therapeutic decisions in axillary node-negative breast cancer. *Annu. Rev. Med.* **44**, 1-10 (1993).

58. Meyer, J. S., Alvarez, C., Milikowski, C., Olson, N., Russo, I., Russo, J., Glass, A., Zehnbauer, B. A., Lister, K. & Parwaresch, R. Breast carcinoma malignancy grading by Bloom-Richardson system vs proliferation index: reproducibility of grade and advantages of proliferation index. *Mod. Pathol.* **18**, 1067–1078 (2005).
59. Robbins, P., Pinder, S., de Klerk, N., Dawkins, H., Harvey, J., Sterrett, G., Ellis, I. & Elston, C. Histological grading of breast carcinomas: A study of interobserver agreement. *Hum. Pathol.* **26**, 873–879 (1995).
60. Rizki, A. & Bissell, M. J. Homeostasis in the breast: It takes a village. *Cancer Cell* **6**, 1–2 (2004).
61. Tambasco, M., Eliasziw, M. & Magliocco, A. M. Morphologic complexity of epithelial architecture for predicting invasive breast cancer survival. *J. Transl. Med.* **8**, 140 (2010).
62. da Silva Júnior, J. G. *et al.* Fractal dimension as tool for vascular diagnosis in health. *Hematol Med Oncol* **4**, 1–4 (2019).
63. Onuchic, A. C. & Chammas, R. Cancer and the tumor microenvironment. *Rev. Med. (São Paulo)* **89**, 21–31 (2010).
64. Ng, C. F. & Frieboes, H. B. Model of vascular desmoplastic multispecies tumor growth. *J. Theor. Biol.* **430**, 245–282 (2017).
65. Lopes-Coelho, F., Martins, F., Pereira, S. A. & Serpa, J. Anti-angiogenic therapy: Current Challenges and Future Perspectives. *Int. J. Mol. Sci.* **22**, 3765 (2021).
66. Baish, J. W. & Jain, R. K. Cancer, angiogenesis and fractals. *Nat. Med.* **4**, 984 (1998).
67. Lee, D. -S., Rieger, H. & Bartha, K. Flow correlated percolation during vascular Remodeling in Growing Tumors. *Phys. Rev. Lett.* **96**, 058104 (2006).
68. Claus, E. B., Chu, P., Howe, C. L., Davison, T. L., Stern, D. F., Carter, D. & DiGiovanna, M. P. Pathobiologic Findings in DCIS of the Breast: Morphologic Features, Angiogenesis, HER-2/neu and Hormone Receptors. *Exp. Mol. Pathol.* **70**, 303–316 (2001).

69. Pribic, J. *et al.* Fractal dimension and lacunarity of tumor microscopic images as prognostic indicators of clinical outcome in early breast cancer. *Biomark. Med.* **9**, 1279–1290 (2015).
70. Ribeiro, F. L., dos Santos, R. V. & Mata, A. S. Fractal dimension and universality in avascular tumor growth. *Phys. Rev. E* **95**, 042406 (2017).
71. Solís-Pérez, J. E., Gómez-Aguilar, J. F. & Atangana, A. A fractional mathematical model of breast cancer competition model. *Chaos Solit. Fractals* **127**, 38–54 (2019).
72. Mombach, J. C. M., Lemke, N., Bodmann, B. E. J. & Idiart, M. A. P. A mean-field theory of cellular growth. *Europhys. Lett.* **59**, 923–928 (2002).
73. d’Onofrio, A. Fractal growth of tumors and other cellular populations: Linking the mechanistic to the phenomenological modeling and vice versa. *Chaos Solit. Fractals* **41**, 875–880 (2009).
74. Yokoyama, T., Kawahara, A., Kage, M., Kojiro, M., Takayasu, H. & Sato, T. Image analysis of irregularity of cluster shape in cytological diagnosis of breast tumors: Cluster analysis with 2D-fractal dimension. *Diagn. Cytopathol.* **33**, 71–77 (2005).
75. Basu, S. Barba, J. & Chan, K. S. Texture Analysis in Cytology Using Fractals. *Proc. SPIE 1153, Applications of Digital Image Processing XII*, 273–284 (1989).
76. Verma, G. *et al.* Microcalcification morphological descriptors and parenchyma fractal dimension hierarchically interact in breast cancer: A diagnostic perspective. *Comput. Biol. Med.* **93**, 1–6 (2018).
77. Kumar, D. & Singh, J. *Fractional Calculus in Medical and Health Science*, CRC Press (2020). <https://doi.org/10.1201/9780429340567>
78. Knutzen, A. M. & Gisvold, J. J. Likelihood of Malignant Disease for Various Categories of Mammographically Detected, Nonpalpable Breast Lesions. *Mayo Clin. Proc.* **68**, 454–460 (1993).

79. Burrell, H. C., Sibbering, D. M., Wilson, A. R., Pinder, S. E., Evans, A. J., Yeoman, L. J., Elston, C. W., Ellis, I. O., Blamey, R. W. & Robertson, J. F. Screening interval breast cancers: mammographic features and prognostic factors. *Radiology* **199**, 811–817 (1996).
80. Banik, S., Rangayyan, R. M. & Desautels, J. E. L. Detection of architectural distortion in prior mammograms using fractal analysis and angular spread of power. *Proc. SPIE 7624, Medical Imaging 2010: Computer-Aided Diagnosis*, 762408 (2010).
81. Bhowmik, M. K., Roy, A., Gogoi, U. R. & Nath, N. Estimation of Architectural Distortion in Mammograms using Fractal Features. *2017 IEEE Nucl. Sci. Symp. Med. Imaging Conf. (NSS/MIC)*, 1-3 (2017).
82. Shanthi, S. & Muralibhaskaran, V. Automatic Detection and Classification of Microcalcification, Mass, Architectural Distortion and Bilateral Symmetry in Digital Mammograms. (2015). 10.5281/zenodo.1337615
83. Dhahbi, S., Barhoumi, W., Kurek, J., Swiderski, B., Kruk, M. & Zagrouba, E. False positive reduction in computer-aided mass detection using mammographic texture analysis and classification. *Comput. Methods Programs Biomed.* **160**, 75–83 (2018).
84. Guliato, D., de Oliveira, W. A. A. & Traina, C. A new feature descriptor derived from Hilbert space-filling curve to assist breast cancer classification. *Proc. - IEEE Symp. Comput. Med. Syst.* 303–308 (2010) doi:10.1109/CBMS.2010.6042660.
85. Klonowski, W., Pierzchalski, M., Stepień, P. & Stepień, R. A. New Fractal Methods for Diagnosis of Cancer. *IFMBE Proc.* **38**, (2013).
86. Uniyal, N. *et al.* Ultrasound RF time series for classification of breast lesions. *IEEE Trans. Med. Imaging* **34**, 652–661 (2015).
87. Ferro, D. P., Falconi, M. A., Adam, R. L., Ortega, M. M., Lima, C. P., de Souza, C. A., Lorand-Metze, I. & Metze, K. Fractal characteristics of May-Grünwald-Giemsa Stained Chromatin Are Independent Prognostic Factors for Survival in Multiple Myeloma. *PLoS One* **6**, e20706 (2011)

88. Soares, F., Janela, F., Pereira, M., Seabra, J. & Freire, M. M. 3D Lacunarity in Multifractal Analysis of Breast Tumor Lesions in Dynamic Contrast-Enhanced Magnetic Resonance Imaging, *IEEE Trans. Image Process.* **22**, 4422-4435 (2013).
89. Horak, E. R. *et al.* Angiogenesis, assessed by platelet/endothelial cell adhesion molecule antibodies, as indicator of node metastases and survival in breast cancer. *Lancet* **340**, 1120–1124 (1992).
90. Goutzanis, L. P. *et al.* Vascular fractal dimension and total vascular area in the study of oral cancer. *Head Neck* **31**, 298-307 (2009).
91. Schneider, D., Tarantola, M. & Janshoff, A. Dynamics of TGF- $\beta$  induced epithelial to mesenchymal transition monitored by Electric Cell-Substrate Impedance Sensing. *Biochim. Biophys. Acta - Mol. Cell Res.* **1813**, 2099–2107 (2011)
92. Waliszewski, P. & Konarski, J. The Gompertzian curve reveals fractal properties of tumor growth. *Chaos Solit. Fractals* **16**, 665–674 (2003).
93. Losa, G. A., Graber, R., Baumann, G. & Nonnenmacher, T. F. Steroid hormones modify nuclear heterochromatin structure and plasma membrane enzyme of MCF-7 cells. A combined fractal, electron microscopical and enzymatic analysis. *Eur. J. Histochem.* **42**, 21-29 (1998).
94. Das, A. *et al.* DNA walk of specific fused oncogenes exhibit distinct fractal geometric characteristics in nucleotide patterns. *Phys. A Stat. Mech. its Appl.* **662**, 130437 (2025).
95. Desper, R., Jiang, F., Kallioniemi, O. P., Moch, H., Papadimitriou, C. H. & Schäffer, A. A. Inferring tree models for oncogenesis from comparative genome hybridization data. *J. Comput. Biol.* **6**, 37–51 (1999).
96. Iurato, G. A proposal for a possible p-adic approach to formally treat molecular biology of certain cancer growth models. (2016). <https://hal.science/hal-01331411v1/file/cancer%20growth%20model.pdf>
97. Su, W. & Qiu, H. p-Adic Calculus and Its Applications To Fractal Analysis and Medical Science. *Facta Univ. - Ser. Electron. Energ.* **21**, 339–347 (2008).



98. Hua, H. & Hovestadt, L. p-adic numbers encode complex networks. *Sci. Rep.* **11**, 17 (2021).
99. Dragovich, B. & Dragovich, A. Y. A p-adic model of DNA sequence and genetic code. *P-Adic Num Ultramet Anal Appl* **1**, 34–41 (2009).
100. Ramos, G. Q., Matos, R. S., Das, A., Kumar, S., Țălu, Ș., & da Fonseca Filho, H. D. Correlating Morphology and Multifractal Spatial Patterns of the Leaf Surface Architecture of *Anacardium occidentale* L. *Fractal Fract.*, **6(6)**, 320 (2022).
101. Xia, Y., Cia, J., Perfect, E., Wei, W., Zhang, Q. & Meng, Q. Fractal dimension, lacunarity and succolarity analyses on CT images of reservoir rocks for permeability prediction. *J. Hydrol.* **579**, 124198 (2019).
102. Cattani, C. & Pierro, G. On the Fractal Geometry of DNA by the Binary Image Analysis. *Bull Math Biol* **75**, 1544–1570 (2013).
103. Devi, S. S. & Vidivelli, S. Modified Differential Box Counting in Breast Masses for Bioinformatics Applications. *Computers, Materials & Continua* **70**, 3049-3066 (2022).
104. Das, A., Bhat, R. & Jolly, M. K. Fractal Measures as Predictors of Histopathological Complexity in Breast Carcinoma Mammograms. *bioRxiv*, (2025). <https://doi.org/10.1101/2025.04.10.648305>
105. Lennon, F. E. *et al.* Lung cancer-a fractal viewpoint. *Nat. Rev. Clin. Oncol.* **12**, 664–675 (2015).

**Acknowledgment:** **A. D.** acknowledges the Department of Biotechnology (DBT)-India for the Research Associate fellowship vide Award Letter No. DBT-RA/2023/January/NE/3594.

**R. B.** acknowledges support from the Indo-French Centre for the Promotion of Advanced Research (69T08-2).

**M. K. J.** acknowledges support from the Param Hansa Philanthropies.

**Declaration of Interest:** The authors declare that they have no known competing financial interests or personal relationships that could have appeared to influence the work reported in this paper.

## Figures

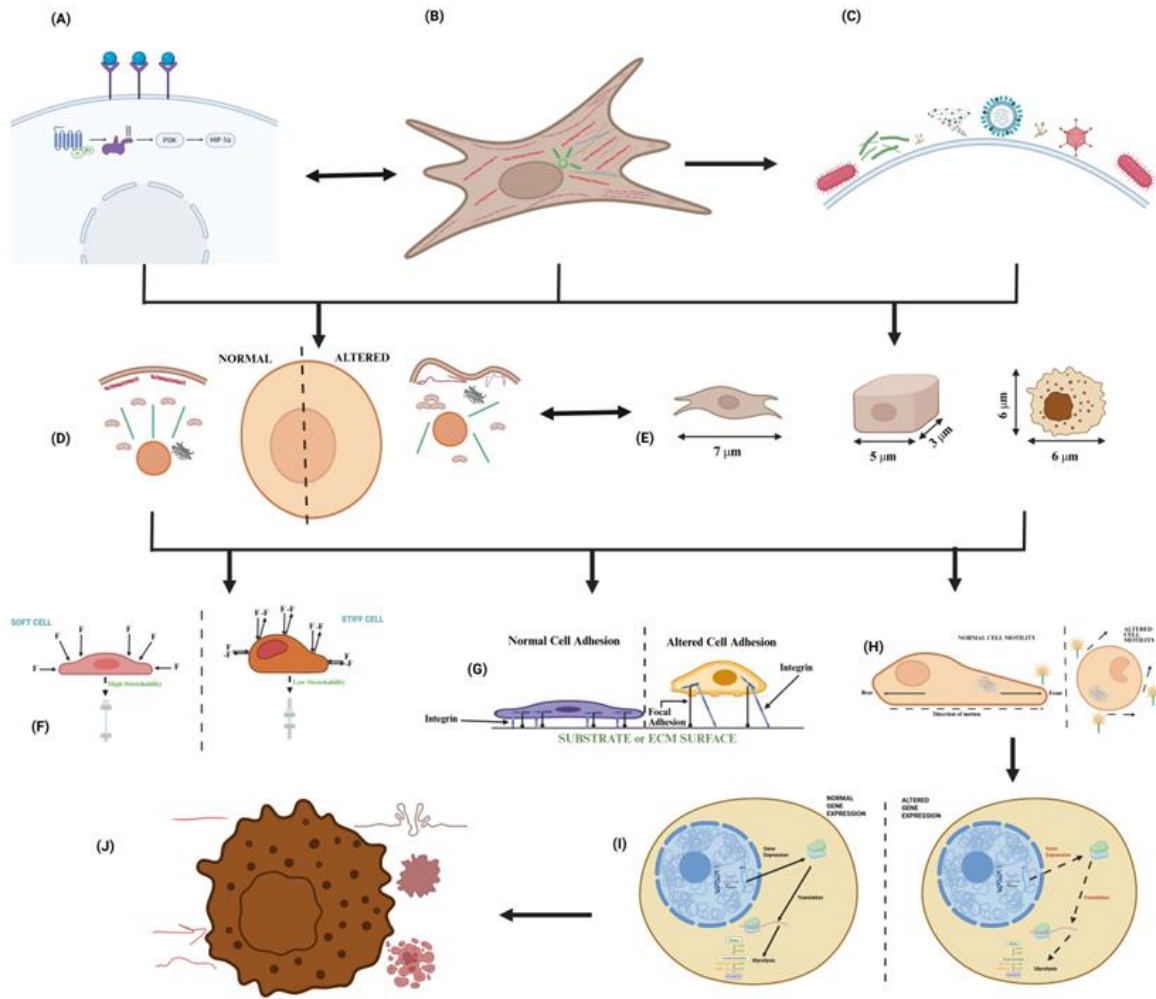


**Fig. 1** Schematic representation of the chemo-biomechanical pathways displaying connection among shape features, cell biomechanics, gene-protein network, cytoskeleton, and disease state. Here, **(A)** Biochemical signals (intracellular or environmental), **(B)** Biophysical constraints/tensional homeostasis, **(C)** Foreign organisms and pathogens, **(D)** Structural changes induced cell membranes, cytoskeleton, and cytosol, **(E)** Variation in cell size and shape, **(F)** Variation in cell deformability, **(G)** Altered cytoadherence, **(H)** Altered cell locomotion and motility, **(I)** Altered cell function and gene expression, and **(J)** Cancerous state

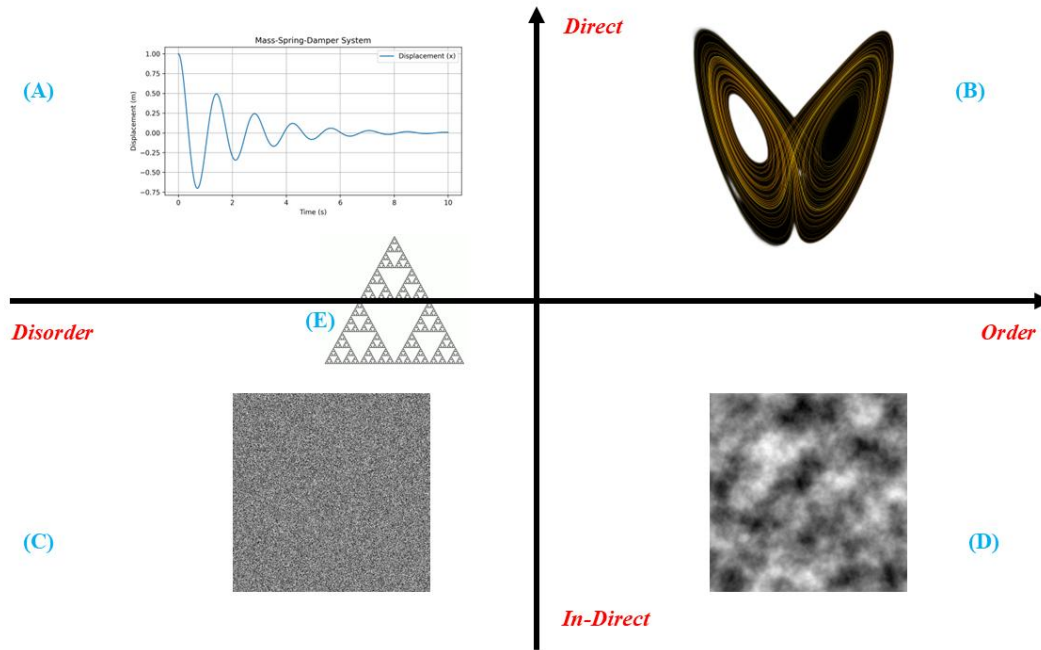


**Fig. 2** Relationship between models/frameworks used for investigating complex dynamical systems. Here, **(A)** Linear time-invariant causal system is represented by the mass-spring-damper system, **(B)** Chaotic system, visually highlighted by the Butterfly effect, **(C)** White noise, **(D)** Turbulence, visually represented by the Perlin noise, and **(E)** Fractals, graphically represented by the Sierpienski triangle

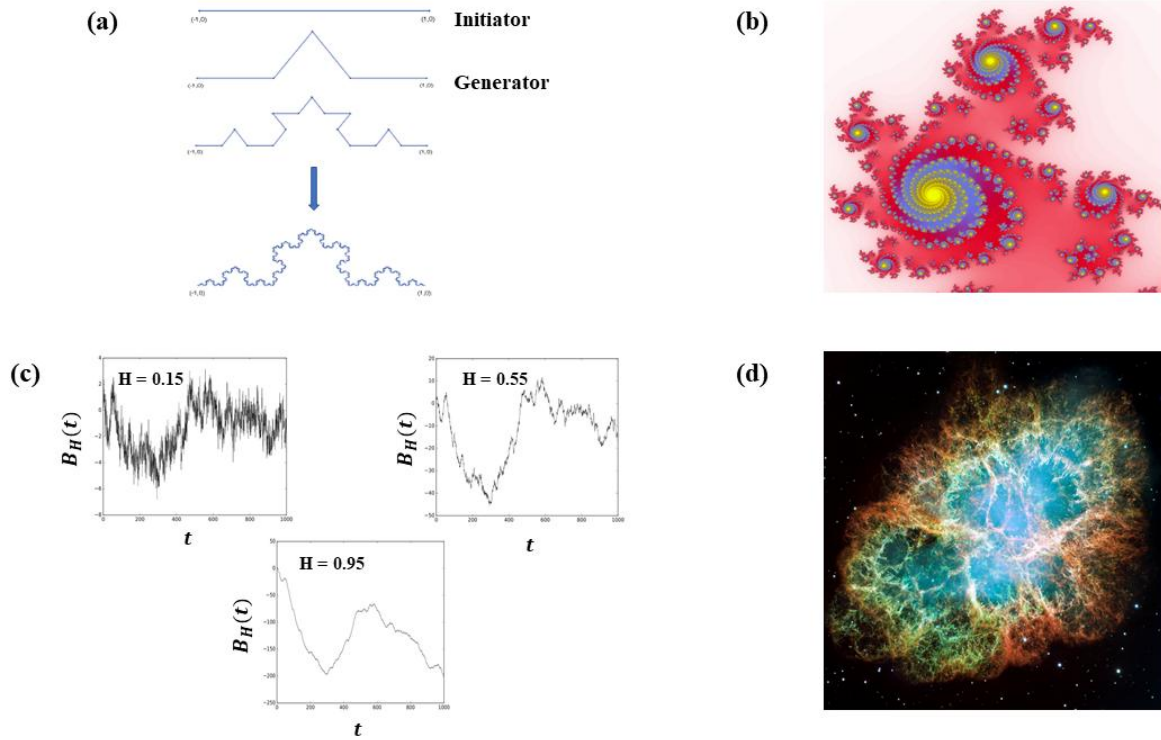


**Fig. 3** (a) Koch curve - Initiator step consists of having a straight line with unit length. In the generator step, the line is divided into three fragments, with the middle third as the base, constructing an equilateral triangle with the removal of the base. The resulting figure consists of  $4^1$  line segments, each with  $1/3^{\text{rd}}$  length, while the total length is  $4/3$ . In the next step, the middle third of each line segment is the base equilateral triangles are constructed with the removal of bases. The resulting figure will have  $4^2$  line segments, with the length of each being  $1/3^2$  such that the total length becomes  $(4/3)^2$ . Successive iterations result in the curve progressively winding with approaching the limiting curve, i.e., the Koch curve, (b) Julia set corresponding to  $0.355 + 0.355i$ , (c) Time trace of particle's position executing fractional Brownian motion with varying Hurst exponent, consequently, displaying persistent, anti-persistent, and no memory-effect, and (d) Crab-nebula, a multi-fractal structure

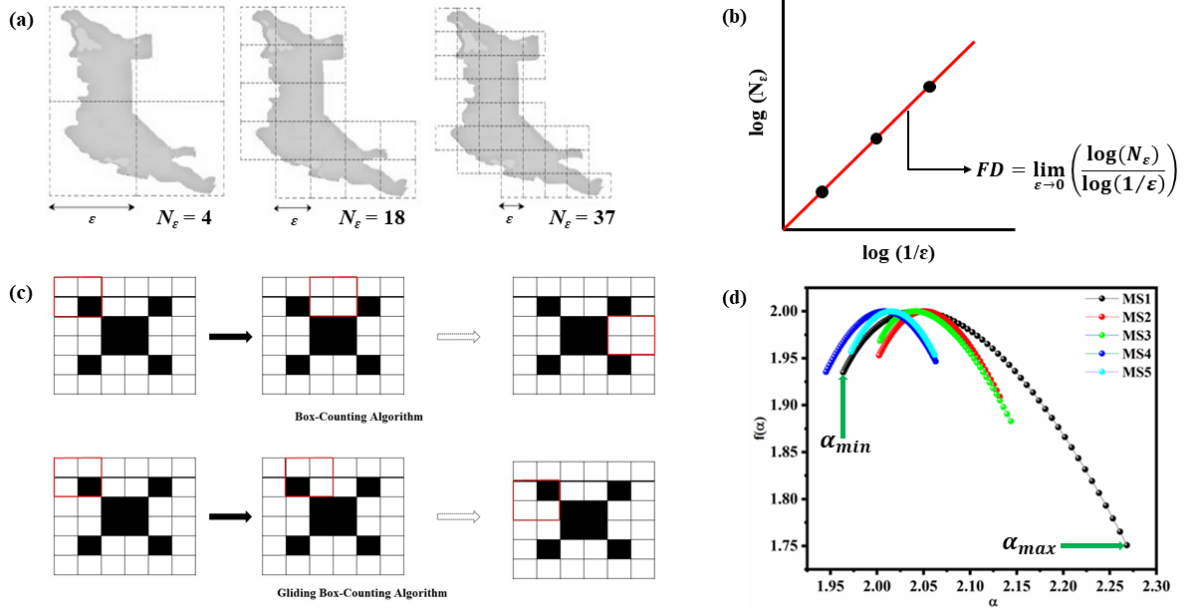


**Fig. 4** Pictorial representation of (a-b) box-counting algorithm for measuring the fractal dimension of an irregular/complex structure and (c) difference between box-counting and gliding box-counting algorithm for computation of fractal dimension and lacunarity, respectively, on a  $6 \times 6$  binary image and (d) Multi-fractal spectrum exhibiting the variation in multifractality strength of sputtered Molybdenum Disulfide thin films with change in thickness<sup>40</sup>